arXiv:cond-mat/0502048v2 [cond-mat.supr-con] 9 May 2005

Dynamics of nonequilibrium quasiparticles in a double superconducting tunnel junction detector

M. Ejrnaes, C. Nappi§, and R. Cristiano

CNR-Istituto di Cibernetica "E. Caianiello", via Campi Flegrei, 34 - Comprensorio "A. Olivetti" - I-80078 Pozzuoli (NA), Italy and
INFN, Complesso Universitario di Monte Sant'Angelo via Cintia, I-80126, Napoli, Italy

Abstract. We study a class of superconductive radiation detectors in which the absorption of energy occurs in a long superconductive strip while the redout stage is provided by superconductive tunnel junctions positioned at the two ends of the strip. Such a device is capable both of imaging and energy resolution. In the established current scheme, well studied from the theoretical and experimental point of view, a fundamental ingredient is considered the presence of *traps*, or regions adjacent to the junctions made of a superconducting material of lower gap. We reconsider the problem by investigating the dynamics of the radiation induced excess quasiparticles in a simpler device, i.e. one without traps. The nonequilibrium excess quasiparticles can be seen to obey a diffusion equation whose coefficients are discontinuous functions of the position. Based on the analytical solution to this equation, we follow the dynamics of the quasiparticles in the device, predict the signal formation of the detector and discuss the potentiality offered by this configuration.

PACS numbers: 85.25.Oj, 85.25.Am, 74.40.+k, 74.50.+r

§ To whom correspondence should be addressed (c.nappi@cib.na.cnr.it)

1. Introduction

Superconducting single photon radiation detectors, such as transition edge sensors microbolometers, superconducting tunnel junctions, kinetic inductance detectors, and superconductive resonator detectors are attractive devices because they have nearly achieved the desired performance for energy-resolved detection of individual photons or particles over a broad energy range with high counting rates [1, 2].

Current work is generally directed towards two objectives: improving energy resolution and scaling to cover large areas. For microbolometers the current trend is to try to multiplex an array of detectors to one readout system. Various techniques have already demonstrated their viability, although several difficulties remain to be solved. The multiplex approach is much more difficult in the case of STJ detectors, as the signals are much faster, thus increasing the bandwidth necessary for the multiplexing circuit. A possibility to simplify the problem is to drastically reduce the number of channels that has to be readout without reducing the number of pixels and the area covered by the array. This can be accomplished by substituting several single pixel STJs in the array with long and narrow strips where radiation is absorbed (as long as possible to cover the largest area). Each strip is readout through two STJs placed at the ends[3, 4, 5]. Such a structure is sometime referred in literature with the acronym DROID which stands for Distributed Read Out Imaging Device [6]. In DROIDs energy resolution is obtained in the same way as for a single STJ by counting the total number of quasiparticles that tunnel through the barriers of the two junctions in time coincident pulses; the position is obtained by measuring the quasiparticles separately collected by the two junctions. The DROID scheme has been demonstrated to give very good position resolution along the absorber strip, and also a good energy resolution[7].

Since the very beginning when DROIDs were proposed, they were designed by using a higher gap superconductor for the absorber and a lower gap superconductor for the STJs electrodes[3]. The idea was to exploit the quasiparticle trapping and the multiplication effects[8] to improve the collection efficiency. In a DROID quasiparticles produced in the absorber after photon absorption will diffuse toward the opposite sides where they are soon trapped and then *counted* by the tunnel junctions. There are currently two different ways on how to realize such *traps* on the sides of the absorber. One places the trap on top of the absorber [3, 6, 9, 10], the other places the trap laterally to the absorber [5, 11]. The first method has the advantage of the best possible interface between the absorber and the trap material as they can be both deposited *in situ* without breaking vacuum during fabrication, but constrains the volume of the trap and junction area severely, and results in STJs affected by the proximity effect. The second has almost no limitations on trap design, and junction area, the STJ are not affected by the proximity effect, but much care must be taken in fabrication to keep the interface between the trap and absorber defect-free. In both designs energy resolution has been measured as degraded because of the temperature rise of the trap when a large amount of quasiparticles enter [12, 13]. This degrades the ability of the

trap to efficiently capture the quasiparticles and increases the dark current of the STJ, which results into a degraded position and energy resolution. The easiest way to remedy this problem is to make bigger traps, if possible, which would reduce the heating effect of the quasiparticles. Apart from the case where the trap volume is constrained by the absorber design, larger traps also means that losses and diffusion inside the traps become relevant phenomena that have to be considered.

In the light of the above considerations, we found the physics of a different DROID design, one that does not use traps, interesting to investigate. The presence of traps is not a fundamental ingredient that underlies the DROID idea. The important issues are the large area coverage with imaging capability and the reduction of the readout channels, while maintaining good energy resolution. Moreover, single pixel STJ detectors have been made without traps; they are well proven examples of detectors that does not have traps but conserve excellent energy resolution[14]. Large area coverage and reduction of readout channels can be kept by simply connecting two STJs to the same bottom electrode (the long absorber) without introducing traps.

A no-trap DROID structure was already analysed in the past [15], but it was not fully appreciated for the advantage of being a simpler structure from several points of view: fabrication technology, diffusion, self-heating. In the model contained in [15] the junctions were considered point-like and were only sensitive to the distribution function of quasiparticles at the edges of the device without any disturbance of the nonequilibrium state in the absorber. In the present work the analysis has been extended to consider the finite size of the junctions, and to include their influence on the nonequilibrium dynamics of excess quasiparticles. In this way the presence of the junctions can determine the detector response.

Finally we remark that the investigation of a DROID structure without traps is also of interest in the perspective, just recently emerged[16], that to obtain STJ-detectors which would be really competitive in terms of energy resolution one will be probably forced to use for the material of the absorber a superconductor with energy gap equal or lower than that of aluminium ($\Delta < 0.18$ meV). The reason is that the ultimate energy resolution in STJs is proportional to the square root of the energy gap of the superconductor where radiation is absorbed. Keeping an energy E = 1 keV as reference for X-ray photons, the intrinsic energy resolution requirement for advanced applications is 2 eV. This is achieved when the energy gap value is equal or less that of the aluminium. Moreover the present state-of-the-art in STJ fabrication technology is based on the Al_2O_3 oxide tunnel barrier, indicating again STJs with Al electrodes as the best and possible choice. It is then natural to consider a whole aluminium DROID, an Al-absorber laterally readout by Al-STJs: definitively a no-trap DROID structure.

In this paper we describe the response of such a detector under the influence of single photons. A model is developed, and an analytic expression is obtained for the evolution in time of the one-dimensional quasiparticle density, from which we calculate the tunnel currents and the collected charge through both the STJs. We discuss the position dependence of the pulse height governed by diffusion and quasiparticles decay.

2. Formulation of the problem

In a superconductor radiation energy is absorbed in a complicated process that results in the generation of an excess number of quasiparticles [17]. A DROID measures the number of nonequilibrium excess quasiparticles as they tunnel through the tunnel junctions positioned at the end of the superconductive absorber. Each junction is polarised at a convenient voltage point in the subgap region of the I-V characteristic. When illuminated, the device provides energy and position information of the incoming radiation by comparing the coincident measured charges in the two junctions. To describe the dynamical behaviour of the proposed detector a model of the spatial and temporal quasiparticle excess density is needed. The structure is schematised in figure 1. It con-

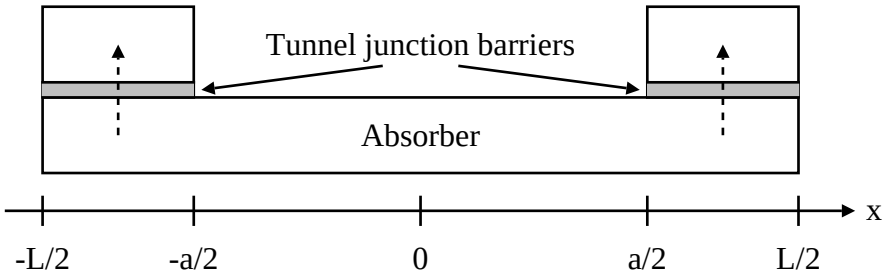

Figure 1. Schematic of the cross section of the proposed detector (not in scale). Dashed arrows on the two sides indicate the excess quasiparticle tunnelling

sists of an absorber of length L, with tunnel junctions at the two edges whose length is $(L-a)/2$. We assume that the effect of the tunnel junctions is to remove the excess quasiparticles created in an impact event of a photon with the absorber with a constant rate probability, $\gamma_{\rm tunn}$, and that the quasiparticles do not re-enter the absorber once removed. We also assume, in the absorber, isotropic diffusion constant, D, and uniform constant loss rate, $\gamma_{\rm loss}$, which accounts for the various mechanism of quasiparticle losses. These assumptions enable us to describe the spatial and temporal evolution of the excess quasiparticle density, $n\left(x,t\right)$, through the standard diffusion equation [4]

$$\frac{\partial n\left(x,t\right)}{\partial t}=D\frac{\partial^{2}n\left(x,t\right)}{\partial x^{2}}-\gamma\left(x\right)n\left(x,t\right),\quad -\mathrm{L}/2<x<\mathrm{L}/2,\quad 0<t<\infty \tag{1}$$

with the boundary conditions

$$\frac{\partial n\left(-L/2,t\right)}{\partial x}=\frac{\partial n\left(L/2,t\right)}{\partial x}=0. \tag{2}$$

The presence of the tunnel junctions is then modelled through $\gamma\left(x\right)=\gamma_{i}$ where the index $i=1,2,3$ refers to the three regions defined as

$$\gamma(x) = \begin{cases} \gamma_1 = \gamma_{\text{loss}} + \gamma_{\text{tunn}} & \text{if -L/2 < x < -a/2} \quad \text{Region 1} \\ \gamma_2 = \gamma_{\text{loss}} & \text{if -a/2 < x < a/2} \quad \text{Region 2} \\ \gamma_3 = \gamma_{\text{loss}} + \gamma_{\text{tunn}} & \text{if a/2 < x < L/2} \quad \text{Region 3} \end{cases} \tag{3}$$

Thus in the two junction regions the probability of tunnelling adds to the probability of loss. Although simple looking, this problem is more complicated compared with that arising when traps are present and, as far as we know, the solution has never been reported. We choose to solve this problem by splitting it into three parts, corresponding to the regions 1, 2, and 3 above. Thus we need to supplement the boundary conditions, Eq. 2, with the requirements that the excess quasiparticle density, and its spatial derivative, are continuous functions at $x = \pm a/2$

$$\begin{array}{c} n_1\left(-\frac{a}{2},t\right) = n_2\left(-\frac{a}{2},t\right),\ n_2\left(\frac{a}{2},t\right) = n_3\left(\frac{a}{2},t\right) \\ \frac{\partial n_1\left(-\frac{a}{2},t\right)}{\partial x} = \frac{\partial n_2\left(-\frac{a}{2},t\right)}{\partial x},\ \frac{\partial n_2\left(\frac{a}{2},t\right)}{\partial x} = \frac{\partial n_3\left(\frac{a}{2},t\right)}{\partial x} \end{array} \tag{4}$$

The radiation impact on the absorber is modeled through the initial condition:

$$n\left(x,0\right) = N_0 \delta\left(x - x_0\right), \tag{5}$$

where x_0 is the radiation impact point and N_0 the number of quasiparticles generated by the radiation impact. All this provides seven relations which together with equation (1) allows to determine the solution in the three domains between $-L/2$ and $L/2$.

3. Solution of the problem

The solution to the problem, equations (1)-(5), can be obtained by the separation of variables method [18] introducing the arbitrary constant ν. Then the unknown density can be written as an integral on all possible values of ν in the three previously defined spatial domains.

$$\begin{aligned} n_i\left(x,t\right) \;=\; & \int_{-\gamma_i}^{0} \mathrm{e}^{-(\gamma_i+\nu_i)t}\left[X_i\left(\nu_i\right)\mathrm{e}^{\sqrt{\frac{-\nu_i}{D}}x} + Y_i\left(\nu_i\right)\mathrm{e}^{-\sqrt{\frac{-\nu_i}{D}}x}\right]\mathrm{d}\nu_i + \\ & + \int_{0}^{\infty} \mathrm{e}^{-(\gamma_i+\nu_i)t}\left[X_i\left(\nu_i\right)\cos\sqrt{\frac{\nu_i}{D}}x + Y_i\left(\nu_i\right)\sin\sqrt{\frac{\nu_i}{D}}x\right]\mathrm{d}\nu_i. \end{aligned} \tag{6}$$

Inserting the full formal solution, equation (6), into the six boundary conditions, see Appendix A, we find that the possible values of ν is an infinite discrete set. It is convenient to distinguish the sign of ν by introducing $\alpha^2 = -D\nu/L^2$ and $\mu^2 = D\nu/L^2$. Then the two equations determining these values of ν, written in terms of α and μ respectively, are

$$\begin{aligned} & \left[\gamma_{\mathrm{D}} + \left(\gamma_{\mathrm{D}} - 2\alpha^2\right)\cosh\left(\alpha - a\alpha\right)\right]\sin\left(a\sqrt{\gamma_{\mathrm{D}} - \alpha^2}\right) + \\ & -2\alpha\sqrt{\gamma_{\mathrm{D}} - \alpha^2}\cos\left(a\sqrt{\gamma_{\mathrm{D}} - \alpha^2}\right)\sinh\left(\alpha - a\alpha\right) = 0 \end{aligned} \tag{7}$$

and

$$\left[\gamma_{\mathrm{D}} + \left(\gamma_{\mathrm{D}} + 2\mu^2\right)\cos\left(\mu - a\mu\right)\right]\sin\left(a\sqrt{\gamma_{\mathrm{D}} + \mu^2}\right) + \\ +2\mu\sqrt{\gamma_{\mathrm{D}} + \mu^2}\cos\left(a\sqrt{\gamma_{\mathrm{D}} + \mu^2}\right)\sin\left(\mu - a\mu\right) = 0, \tag{8}$$

where $\gamma_{\mathrm{D}} = \gamma_{\mathrm{tunn}} L^2/D$. Once the possible values of the constant ν have been determined the two integrals in equation (6) change into sums. Thus equation (6) can be written as

$$n_i\left(x,\tau\right) = \sum_{n=0}^{N_\alpha - 1} R_n\left(\alpha_n, x_0\right) \mathrm{e}^{-\left(\frac{\gamma_i}{\gamma_{\mathrm{loss}}} - \alpha_n^2 \frac{\Lambda^2}{L^2}\right)\tau} F_{i,n}\left(\alpha_n, x\right) + \\ + \sum_{n=N_\alpha}^{\infty} S_n\left(\mu_n, x_0\right) \mathrm{e}^{-\left(\frac{\gamma_i}{\gamma_{\mathrm{loss}}} + \mu_n^2 \frac{\Lambda^2}{L^2}\right)\tau} G_{i,n}\left(\mu_n, x\right) \tag{9}$$

where α_n, μ_n are solutions to equations (7) and (8), respectively, and the two proportionality constants $R_n\left(\alpha_n, x_0\right)$ and $S_n\left(\mu_n, x_0\right)$ will be determined by the initial condition. We have also introduced the normalised time, $\tau = t\gamma_{\mathrm{loss}}$, the finite number of possible α-values, N_α (see Appendix A), the diffusion length $\Lambda = \sqrt{D/\gamma_{\mathrm{loss}}}$, and the spatial base functions

$$F_{i,n}\left(\alpha_n, x\right) = \begin{cases} A_{i,n}\left(\alpha_n\right)\mathrm{e}^{\alpha_n x} + B_{i,n}\left(\alpha_n\right)\mathrm{e}^{-\alpha_n x} & , \, i = 1,3 \\ A_{i,n}\left(\alpha_n\right)\cos\left(\sqrt{\gamma_D - \alpha_n^2}x\right) + B_{i,n}\left(\alpha_n\right)\sin\left(\sqrt{\gamma_D - \alpha_n^2}x\right) & , \, i = 2 \end{cases} \tag{10}$$

$$G_{i,n}\left(\mu_n, x\right) = \begin{cases} C_{i,n}\left(\mu_n\right)\cos\left(\mu_n x\right) + D_{i,n}\left(\mu_n\right)\sin\left(\mu_n x\right) & , \, i = 1,3 \\ C_{i,n}\left(\mu_n\right)\cos\left(\sqrt{\gamma_D + \mu_n^2}x\right) + D_{i,n}\left(\mu_n\right)\sin\left(\sqrt{\gamma_D + \mu_n^2}x\right) & , \, i = 2 \end{cases} \tag{11}$$

in which all lengths (x, x_0, a) are normalised to L, unless otherwise indicated. The procedure to obtain the coefficients $A_{i,n}, B_{i,n}, C_{i,n}, D_{i,n}, R_n, S_n$ is described in detail in Appendix B along with their analytical expressions.

At this point the mathematical problem is completely solved, and the spatial and temporal response of the proposed detector is known. An example of the spatial evolution of the density of excess quasiparticles in an aluminium device is shown in figure 2 at subsequent instants of time (in units of γ_{loss}) for an event occurred at $x_0 = 0.3$. We used values of the parameters which are compatible with those of a device based on aluminium: $D = 60$ cm^2/s, $\gamma_{\mathrm{loss}} = 10^4$ s^{-1}, $\Lambda = 775$ μm, $L = 775$ μm, for the absorber, and a tunnelling rate $\gamma_{\mathrm{tunn}} = 1.43 \times 10^6$ s^{-1} for the two junctions, each long 50 μm, ($a = 675$ μm, in absolute units). Note that no trace remains, in the time evolving density, of the discontinuity in the coefficient $\gamma(x)$ so that the transition between the absorber and the junction regions is completely smooth.

4. Analysis of the detector signal

To show the potential of the result obtained in the previous section, we will calculate the signals that are typically measured in experiments with DROIDs (i.e. tunnelling current pulses flowing through the junctions). These currents are calculated as

$$I_1\left(x_0, \tau\right) = \gamma_{\mathrm{tunn}} e L \int_{-\frac{1}{2}}^{-\frac{a}{2}} n\left(x, \tau\right) \mathrm{d}x \tag{12}$$

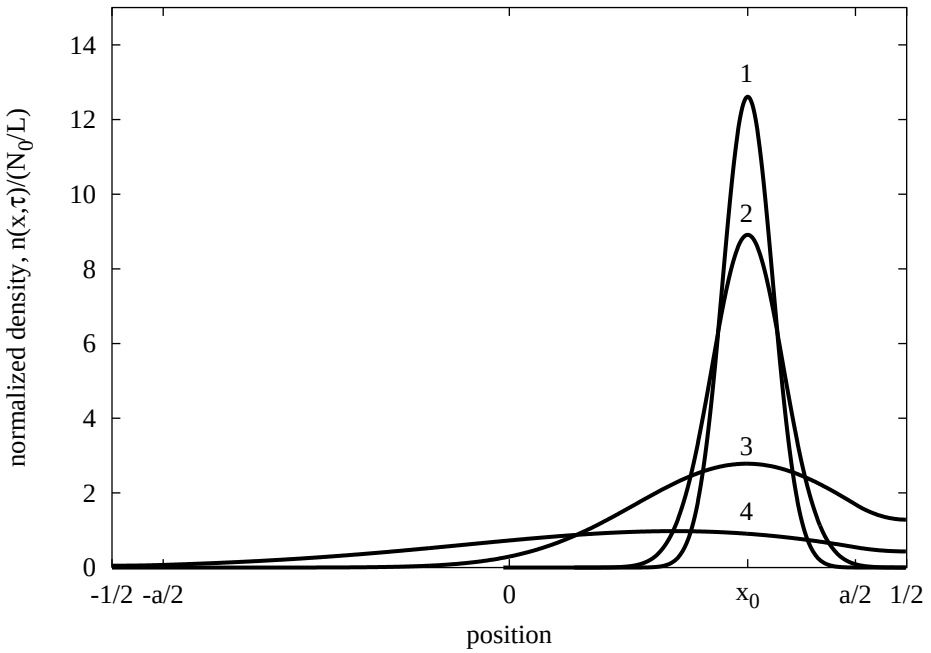

Figure 2. Temporal evolution of the density of excess quasiparticles in the device for an event occurring at $x_0 = 0.3$. Curves $1, 2, 3, 4$ correspond to $\tau = t\gamma_{\rm loss} = 0.0005, 0.001, 0.01, 0.5$. The parameters used are $\Lambda/L = 1$, $\gamma_{\rm tunn}/\gamma_{\rm loss} = 143$, $a = 0.87$

$$I_2\left(x_0,\tau\right) = \gamma_{\rm tunn} eL \int_{\frac{a}{2}}^{\frac{1}{2}} n\left(x,\tau\right) \mathrm{d}x \tag{13}$$

and are given by the expressions

$$\begin{aligned} I_1\left(x_0,\tau\right) = {} & \gamma_{\rm tunn} eL \sum_{n=0}^{N_\alpha - 1} \frac{R_n\left(\alpha_n, x_0\right)}{\alpha_n} \mathrm{e}^{-\left(\frac{\gamma_1}{\gamma_{\rm loss}} - \alpha_n^2 \frac{\Lambda^2}{L^2}\right)\tau} \left(\mathrm{e}^{\frac{\alpha_n}{2}} - \mathrm{e}^{\frac{a\alpha_n}{2}}\right) \left(A_{1,n} \mathrm{e}^{-\alpha_n \frac{1+a}{2}} + B_{1,n}\right) \\ & + \gamma_{\rm tunn} eL \sum_{n=N_\alpha}^{\infty} \frac{S_n\left(\mu_n, x_0\right)}{\mu_n} \mathrm{e}^{-\left(\frac{\gamma_1}{\gamma_{\rm loss}} + \mu_n^2 \frac{\Lambda^2}{L^2}\right)\tau} \times \\ & \times \left\{ D_{1,n} \left[\cos\left(\frac{\mu_n}{2}\right) - \cos\left(\frac{a\mu_n}{2}\right)\right] + C_{1,n} \left[\sin\left(\frac{\mu_n}{2}\right) - \sin\left(\frac{a\mu_n}{2}\right)\right]\right\} \end{aligned} \tag{14}$$

$$\begin{aligned} I_2\left(x_0,\tau\right) = {} & \gamma_{\rm tunn} eL \sum_{n=0}^{N_\alpha - 1} \frac{R_n\left(\alpha_n, x_0\right)}{\alpha_n} \mathrm{e}^{-\left(\frac{\gamma_1}{\gamma_{\rm loss}} - \alpha_n^2 \frac{\Lambda^2}{L^2}\right)\tau} \left(\mathrm{e}^{\frac{\alpha_n}{2}} - \mathrm{e}^{\frac{a\alpha_n}{2}}\right) \left(B_{3,n} \mathrm{e}^{-\alpha_n \frac{1+a}{2}} + A_{3,n}\right) \\ & + \gamma_{\rm tunn} eL \sum_{n=N_\alpha}^{\infty} \frac{S_n\left(\mu_n, x_0\right)}{\mu_n} \mathrm{e}^{-\left(\frac{\gamma_1}{\gamma_{\rm loss}} + \mu_n^2 \frac{\Lambda^2}{L^2}\right)\tau} \times \\ & \times \left\{ D_{3,n} \left[\cos\left(\frac{a\mu_n}{2}\right) - \cos\left(\frac{\mu_n}{2}\right)\right] + C_{3,n} \left[\sin\left(\frac{\mu_n}{2}\right) - \sin\left(\frac{a\mu_n}{2}\right)\right]\right\} \end{aligned} \tag{15}$$

Figure 3 shows the two current pulses for the absorption event shown in figure 2. In literature one typically finds expressions for the collected charges at the two lateral sides

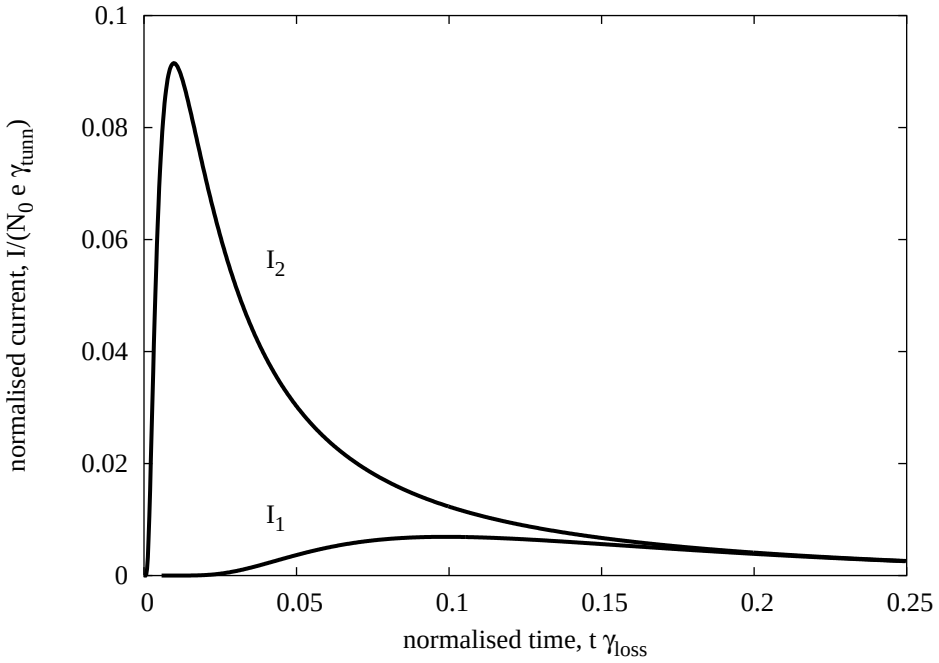

Figure 3. Temporal evolution of the normalised currents passing through the tunnel junctions for the absorption event located at $x_0 = 0.3$. Parameters correspond to $\Lambda/L = 1$, $\gamma_{\rm tunn}/\gamma_{\rm loss} = 143$, $a = 0.87$

of the absorber, which were directly derived through equations governing the charge itself [4] rather than the density. We emphasise that to fully characterise the DROID behaviour it is certainly of great help to also have expressions for the extra tunnelling currents as those calculated above, which is possible only when the solution for $n(x,t)$ has been obtained as we did here.

Finally the collected charge in each tunnel junction as a function of the impact point x_0 can be calculated as

$$Q_{1,2}\left(x_0\right) = \int_0^\infty I_{1,2}\left(x_0, t\right) \mathrm{d}t. \tag{16}$$

and is given by the expressions:

$$\begin{aligned} Q_1\left(x_0\right) = \frac{\gamma_{\rm tunn}}{\gamma_{\rm loss}} eL \sum_{n=0}^{N_\alpha - 1} \frac{R_n\left(\alpha_n, x_0\right)}{\alpha_n \left(\frac{\gamma_1}{\gamma_{\rm loss}} - \alpha_n^2 \frac{\Lambda^2}{L^2}\right)} \left(\mathrm{e}^{\frac{\alpha_n}{2}} - \mathrm{e}^{\frac{a\alpha_n}{2}}\right) \left(A_{1,n} \mathrm{e}^{-\alpha_n \frac{1+a}{2}} + B_{1,n}\right) \\ + \frac{\gamma_{\rm tunn}}{\gamma_{\rm loss}} eL \sum_{n=N_\alpha}^{\infty} \frac{S_n\left(\mu_n, x_0\right)}{\mu_n \left(\frac{\gamma_1}{\gamma_{\rm loss}} + \mu_n^2 \frac{\Lambda^2}{L^2}\right)} \left\{ D_{1,n} \left[\cos\left(\frac{\mu_n}{2}\right) - \cos\left(\frac{a\mu_n}{2}\right)\right] + \right. \\ \left. + C_{1,n} \left[\sin\left(\frac{\mu_n}{2}\right) - \sin\left(\frac{a\mu_n}{2}\right)\right] \right\} \end{aligned} \tag{17}$$

$$Q_2\left(x_0\right) = \frac{\gamma_{\rm tunn}}{\gamma_{\rm loss}} eL \sum_{n=0}^{N_\alpha - 1} \frac{R_n\left(\alpha_n, x_0\right)}{\alpha_n \left(\frac{\gamma_1}{\gamma_{\rm loss}} - \alpha_n^2 \frac{\Lambda^2}{L^2}\right)} \left(\mathrm{e}^{\frac{\alpha_n}{2}} - \mathrm{e}^{\frac{a\alpha_n}{2}}\right) \left(B_{3,n} \mathrm{e}^{-\alpha_n \frac{1+a}{2}} + A_{3,n}\right)$$

$$+\frac{\gamma_{\rm tunn}}{\gamma_{\rm loss}}eL\sum_{n=N_\alpha}^{\infty}\frac{S_n\left(\mu_n,x_0\right)}{\mu_n\left(\frac{\gamma_1}{\gamma_{\rm loss}}+\mu_n^2\frac{\Lambda^2}{L^2}\right)}\left\{D_{3,n}\left[\cos\left(\frac{a\mu_n}{2}\right)-\cos\left(\frac{\mu_n}{2}\right)\right]+\right.$$
$$\left.+C_{3,n}\left[\sin\left(\frac{\mu_n}{2}\right)-\sin\left(\frac{a\mu_n}{2}\right)\right]\right\} \quad (18)$$

Through equations (17),(18) curves at constant energy and constant absorption positions can be constructed (see next section) for a direct comparison with the typical experimental data representation [3, 4].

5. Results and discussion

The behaviour of a DROID is often analysed by plotting coincident collected charges (Q_1, Q_2) for all the possible values of x_0 at constant energy (i.e. constant N_0). Following this choice, in figure 4a we show the response of the no-trap-DROID (equations (17) and (18)) for various values of Λ/L corresponding to absorbers with different values of the diffusion constant D or different values of the loss rate $\gamma_{\rm loss}$. The initial and the final points of each curve, where charge maximises, correspond always to the $-L/2$ and $L/2$ positions on the absorber. Therefore spatial resolution scales inversly with charge collected in these points. It is seen that increasing Λ/L, simultaneously increases the charge yield, makes the charge yield more uniform (the curve shape becomes more straight) and reduces the spatial resolution (the total extension of the curve shortens). In the limit of very efficient diffusion (curve 4), the spatial resolution is lost and the response becomes similar to that of a single STJ. Figure 4b shows the no-trap-DROID response for increasing values of $\gamma_{\rm tunn}/\gamma_{\rm loss}$, corresponding to devices with increasing tunnel junction transparencies. In this case the charge yield, the uniformity of the charge yield and spatial resolution of the device simultaneously increase. Curve 3 in figure 4a and curve 4 in figure 4b coincide and refer to the same device considered in figure 2 and 3. We stress that these curves predict a behaviour comparable to that of a DROID based on the quasiparticle trapping principle [4, 5] and that all the essential features of this last device are conserved in the device described here.

It is also of interest to briefly discuss the role of the junction size by investigating the role of the geometrical parameter a. This can be done by using the same type of Q_1, Q_2 plot as before by simply emphasising points corresponding to the same equidistant positions of radiation absorption. Two such curves are shown in figure 5 in which the open circles, superimposed to the solid line, mark the points corresponding to an arbitrary segmentation of the device in twenty equal intervals. The lower curve, curve 1, has $a = 0.95$, the higher, curve 2, has $a = 0.5$, moreover $\gamma_{\rm tunn}/\gamma_{\rm loss} = 143$, $\Lambda/L = 1$; the geometry of the devices corresponding to these curves are sketched in the inset of the same figure (the gray regions indicate the junctions). A smaller a value (larger junctions) results in an increased charge yield with larger uniformity. Furthermore the spatial resolution is strongly nonuniform as indicated by the lateral crowding, and the simultaneous central rarefaction of points. Therefore the DROID becomes very position sensitive in the central region while under the junctions this sensitivity is degraded. To

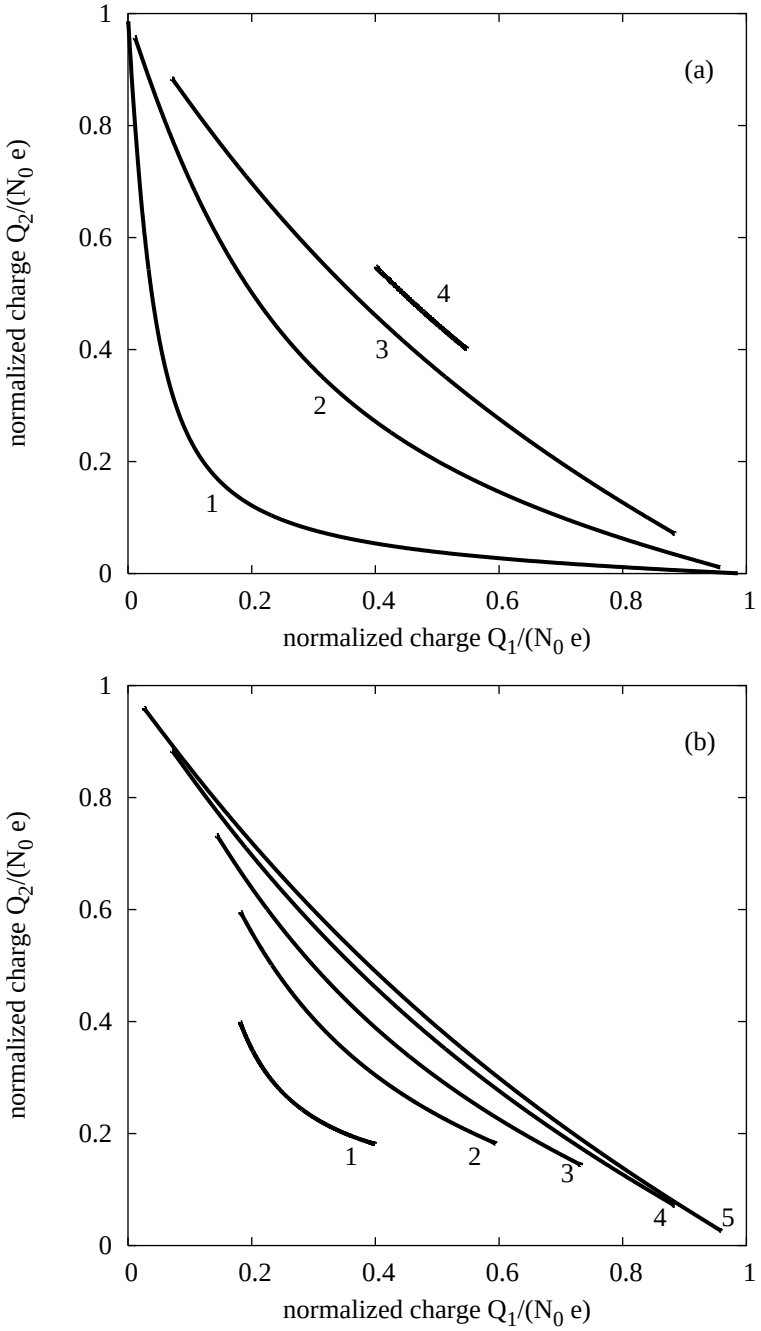

Figure 4. *a*) Collected charges Q_2 vs Q_1 for increasing values of $\Lambda/L, (0.25, 0.5, 1.0, 5.0), \gamma_{\rm tunn}/\gamma_{\rm loss} = 143$ and $a = 0.871$. *b*) Collected charges Q_2 vs Q_1 for increasing values of $\gamma_{\rm tunn}/\gamma_{\rm loss}$, $(10.0, 25.0, 50.0, 143.0, 400.0)$, $\Lambda/L = 1$,$a = 0.871$

better illustrate this effects, in figure 5, we indicated two points (solid circle) on each curve corresponding to the same impinging radiation position (arbitrarily chosen) on the two detectors and marked in the inset by arrows.

In conclusion we have analysed in detail the behaviour of a class of superconductive radiation detectors, denominated DROID, in which the absorption of energy occurs in a long superconductive strip and the readout stage is provided by superconducting tunnel junctions positioned at the two ends of the strip. We have introduced boundary conditions suitable for the absence of trapping regions and solved analytically the resulting diffusion problem. We underline that the model provides not only the total charges collected by the two junctions but also explicit expressions for the tunnelling current pulses. Our analysis shows that a device based on a single superconductive material (i.e. without traps) is still capable both of position and energy resolution. Recently, aluminium has been proposed as the material of choice to achieve the best energy resolution and imaging is obtained by arrays of single superconducting tunnel junctions. Unless other considerations are put forward, our work demonstrates the feasibility of an alternative viable solution to imaging, i.e the DROID configuration, which can be entirely based on a single material, e.g. aluminium.

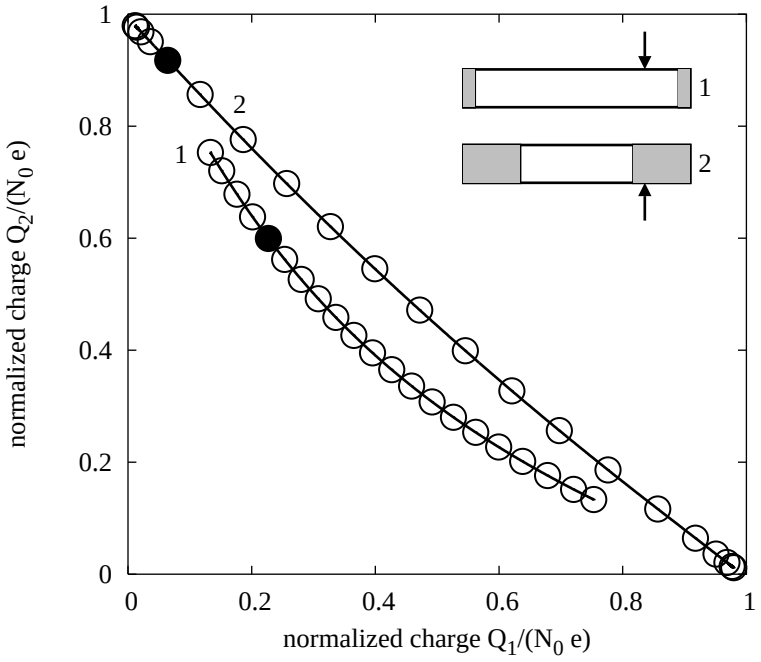

Figure 5. Detector response for two different values of the geometrical parameter a (the size of the junction-free region of the device). Curve 1, a device with $a = 0.95$, curve 2 a device with $a = 0.5$. In the inset, a sketch of the two detectors corresponding to the two curves. The gray regions indicate the junctions. Open circles indicate signals coming from equi-spaced and uniformly distributed positions along the device. The two solid circles are signals coming from the position marked by the arrows on the two devices

6. Acknowledgements

This work has been partially supported by the EC-RTM Network *Applied Cryodetectors* contract no. HPRNCT2002000322 and Progetto FIRB n. RBNE01KJHT.

References

[1] LTD-10 volume *Nucl. Instrum. and Methods A* 2004 **520**

[2] V. Polushkin, 2004 *Nuclear Electronics: Superconducting Detectors and Processing Techniques* (Wiley),

[3] H. Kraus, F.v. Feilitzsch, J. Jochum, R.L. Mossbauer, Th. Peterreins and F. Probst, 1989 *Phys. Letts. B* **234** 195

[4] J. Jochum, H. Kraus, M. Gutsche, B. Kemmather, F. v. Feilitzsch, R.L. Mössbauer 1993 *Ann. Physik* , **2**, 611

[5] S. Friedrich, K. Segall, M.C.Gaidis, C.M.Wilson, D.E. Prober A. E. Szymkowiak, S.H.Moseley, 1997 *Appl. Phys. Lett.* **71** 3901-3903

[6] R. den Hartog, D. Martin, A. Kozorezov, P. Verhoeve, N. Rando, A. Peacock, G. Brammertz, M. Krumrey, D. Goldie, R. Venn ESA Preprint, ESLAB 2000/018/SA in Proceeding of SPIE 2000, 27-31 March 2000 Munich, Germany

[7] L.Li, L. Frunzio, C. Wilson, D. E. Prober, A. E. Szymkowiak, S.H.Moseley, 2001 *J. Appl. Phys.* **90** 3645

[8] N.E. Booth 1987 *Appl. Phys.Letts.* **50** 293

[9] Th. Nussbaumer, Ph. Lerch, E. Kirk, and A. Zehnder R. Fuchslin and P. F. Meier, H. R. Ott, 2000 *Phys. Rev. B* **61** 9721-9728

[10] P. Feautrier C. Jorel, J. C. Villegier B. Delaët E. Lecoarer, A. Benoit *Proceedings of 9th International Workshop on Low temperature detectors, LTD-9* AIP Conference Series vol. 605 NY 2002, p.153

[11] M.P. Lissitski, D. Perez de Lara, R. Cristiano, M.L. Della Rocca, L. Maritato, M. Salvato 2004 *Nucl. Instrum. Methods NIM A* **520** 243-245

[12] K. Segall, C. Wilson, L. Frunzio, L. Li, S. Friedrich, M. C. Gaidis, D. E. Prober, A. E. Szymkowiak, and S. H. Moseley 2000 *Appl. Phys. Lett.* **76** 3998

[13] A. G. Kozorezov, J. K. Wigmore, A. Peacock, R. den Hartog, D. Martin, G. Brammertz, P. Verhoeve, and N. Rando 2004 *Phys. Rev. B* **69** 184506

[14] G. Angloher, P. Hettl, M. Huber, J. Jochum, F.V. Feilitzsch, R.L. Mossbauer, 2001 *J. Appl. Phys.* **89**, 1425-1429

[15] E. Esposito, B. Ivlev, G. Pepe, U. Scotti di Uccio 1994, *J. Appl. Phys.* **76** 1291

[16] G. Brammertz, P. Verhoeve, D. Martin, A. Peacock, R. Venn, ESA Preprint, 2004/SCI-A/024 to be published in Proceeding of SPIE 2000, 21-25 June 2004 Glasgow, UK

[17] A. G. Kozorezov, A. F. Volkov, J. K. Wigmore, A. Peacock, A. Poelaert, and R. den Hartog 2000 *Phys. Rev. B* **61** 11807

[18] W.E. Williams 1980 *Partial Differential Equations* (Clarendon Press), Oxford

Appendix A. Matrix coefficients

Inserting the full formal solution, equation (6), into the six boundary conditions, equation (2), and using the substitutions $\nu_1 = \nu_3 = \nu$ and $\nu_2 = \nu + \gamma_{\text{tunn}}$, it is found that time-independence of the boundary conditions splits the set of equations for $X_1, Y_1, X_2, Y_2, X_3, Y_3$ into three sets, depending on the value of ν. The first set of equations, for the values $-\gamma_{\text{tunn}} - \gamma_{\text{loss}} < \nu < -\gamma_{\text{tunn}}$, arises from matching exponential functions in region 1 and 3 with exponential functions in region 2. The second set of equations, for the values $-\gamma_{\text{tunn}} < \nu < 0$, arises from matching exponential functions in region 1 and 3 with the trigonometric functions in region 2. The last set of equations, for positive values of ν, arises from matching trigonometric functions in region 1 and 3 with trigonometric functions in region 2. Despite the differences between the three sets of equations it is possible to write them in the same matrix form

$$\begin{bmatrix} m_{11} & m_{12} & 0 & 0 & 0 & 0 \\ m_{21} & m_{22} & m_{23} & m_{24} & 0 & 0 \\ m_{31} & m_{32} & m_{33} & m_{34} & 0 & 0 \\ 0 & 0 & m_{43} & m_{44} & m_{45} & m_{46} \\ 0 & 0 & m_{53} & m_{54} & m_{55} & m_{56} \\ 0 & 0 & 0 & 0 & m_{65} & m_{66} \end{bmatrix} \times \begin{bmatrix} X_1 \\ Y_1 \\ X_2 \\ Y_2 \\ X_3 \\ Y_3 \end{bmatrix} = \begin{bmatrix} 0 \\ 0 \\ 0 \\ 0 \\ 0 \\ 0 \end{bmatrix} \tag{A.1}$$

The exact expression of the matrix elements $m_{i,j}$ depends on the three possible ranges of values of ν. They are listed in Table (A1), written in terms of $\alpha^2 = -D\nu/L^2$ and $\mu^2 = D\nu/L^2$. Inspection of the determinants of the three matrices shows that for $-\gamma_{\text{tunn}} - \gamma_{\text{loss}} < \nu < -\gamma_{\text{tunn}}$ only the trivial solution exists. On the contrary, non-trivial solutions can be found for a finite number, N_α, of values of ν when the interval $-\gamma_{\text{tunn}} < \nu < 0$ is considered (solutions to equation (7)), and also for an infinite discrete set of values of ν for $\nu > 0$ (solutions to equation (8)). These two equations express the conditions for theexitancee of non-trivial solutions in the two considered intervals of ν.

Table A1. Expressions in terms of α and μ of the matrix elements appearing in eq. (A.1). ($\alpha^2 = -D\nu/L^2$ and $\mu^2 = D\nu/L^2$).

Element	$-\gamma - \gamma_t < \nu < -\gamma_t$	$-\gamma_t < \nu < 0$	$\nu > 0$
m_{11}	$\exp\left(-\frac{\alpha}{2}\right)$	$\exp\left(-\frac{\alpha}{2}\right)$	$\sin\left(\frac{\mu}{2}\right)$
m_{12}	$-\exp\left(\frac{\alpha}{2}\right)$	$-\exp\left(\frac{\alpha}{2}\right)$	$\cos\left(\frac{\mu}{2}\right)$
m_{21}	$\exp\left(-\frac{a\alpha}{2}\right)$	$\exp\left(-\frac{a\alpha}{2}\right)$	$\cos\left(\frac{a\mu}{2}\right)$
m_{22}	$\exp\left(\frac{a\alpha}{2}\right)$	$\exp\left(\frac{a\alpha}{2}\right)$	$-\sin\left(\frac{a\mu}{2}\right)$
m_{23}	$-\exp\left(-\frac{a\sqrt{\alpha^2-\gamma_D}}{2}\right)$	$-\cos\left(\frac{a\sqrt{\gamma_D-\alpha^2}}{2}\right)$	$-\cos\left(\frac{a\sqrt{\gamma_D+\mu^2}}{2}\right)$
m_{24}	$-\exp\left(\frac{a\sqrt{\alpha^2-\gamma_D}}{2}\right)$	$\sin\left(\frac{a\sqrt{\gamma_D-\alpha^2}}{2}\right)$	$\sin\left(\frac{a\sqrt{\gamma_D+\mu^2}}{2}\right)$
m_{31}	αm_{21}	αm_{21}	$-\mu m_{22}$
m_{32}	$-\alpha m_{22}$	$-\alpha m_{22}$	μm_{21}
m_{33}	$\sqrt{\alpha^2-\gamma_D}m_{23}$	$-\sqrt{\gamma_D-\alpha^2}m_{24}$	$-\sqrt{\gamma_D+\mu^2}m_{24}$
m_{34}	$-\sqrt{\alpha^2-\gamma_D}m_{24}$	$\sqrt{\gamma_D-\alpha^2}m_{23}$	$\sqrt{\gamma_D+\mu^2}m_{23}$
m_{43}	$\sqrt{\alpha^2-\gamma_D}m_{24}$	$\sqrt{\gamma_D-\alpha^2}m_{24}$	$\sqrt{\gamma_D+\mu^2}m_{24}$
m_{44}	$-\sqrt{\alpha^2-\gamma_D}m_{23}$	$\sqrt{\gamma_D-\alpha^2}m_{23}$	$\sqrt{\gamma_D+\mu^2}m_{23}$
m_{45}	αm_{22}	αm_{22}	μm_{22}
m_{46}	$-\alpha m_{21}$	$-\alpha m_{21}$	μm_{21}
m_{53}	m_{24}	m_{23}	m_{23}
m_{54}	m_{23}	$-m_{24}$	$-m_{24}$
m_{55}	m_{22}	m_{22}	m_{21}
m_{56}	m_{21}	m_{21}	$-m_{22}$
m_{65}	$-m_{12}$	$-m_{12}$	$-m_{11}$
m_{66}	$-m_{11}$	$-m_{11}$	m_{12}

Appendix B. Coefficients in the solution, equation (9)

As the problem is symmetric in space the spatial modes separate in even and odd modes. The first mode is even, the second odd and so on. This means that the symmetry of the first mode in the second sum in equation (9) depends on whether N_α is even or odd (which is why we have chosen to let is start from N_α instead of from 0). Insight into when a mode leaves the second sum in equation (9) and appears in the first sum is obtained by examining equation 8 in the limit $\mu \to 0$. It is found that equation 8 reduces to $\sin\left(a\sqrt{\gamma_{\mathrm{D}}}\right) = 0$. From this limit it is easily seen that it is possible to express N_α as the smallest integer greater than $a\sqrt{\gamma_{\mathrm{D}}}/\pi$.

We obtain exact expressions for the even coefficients ($A_{i,2n}$ and $B_{i,2n}$) by assuming $A_{2,2n}$ known. Then we create a reduced system of five equations with five unknowns by moving all the terms containing $A_{2,n}$ to the right hand side in equation (A.1) and eliminate a row (exactly which one is not important as the six rows arelinearlyy dependent on each other). By solving this system of equations we obtain $A_{i,2n}$ and $B_{i,2b}$ except for a proportional constant, $R_n(\alpha_n, x_0)$ in equation (9), which will be determined using the initial condition (equation (5)). Care should be taken as the expressions obtained are not valid for the odd coefficients ($A_{i,2n+1}$ and $B_{i,2n+1}$) because for these coefficients $A_{2,2n+1}$ is zero and thus creates problems when selected as known. We instead select $B_{2,2n+1}$ as known and repeat the procedure as above. Likewise for the second sum in equation (9) we select first $C_{2,2n}$ as known to obtain the even coefficients and then select $D_{2,2n+1}$ as known to obtain the odd coefficients. Also for the these coefficients we have to determine a proportional constant, $S_n(\mu_n, x_0)$ in equation (9), using equation (5). The expressions obtained are:

$$A_{1,n}(\alpha_n) = \exp\left(\alpha_n + \frac{a\alpha_n}{2}\right)\sqrt{\gamma_D - \alpha_n^2} \tag{B.1}$$

$$B_{1,n}(\alpha_n) = \exp\left(\frac{a\alpha_n}{2}\right)\sqrt{\gamma_D - \alpha_n^2} \tag{B.2}$$

$$C_{1,n}(\mu_n) = \sqrt{\gamma_D + \mu_n^2}\cos\left(\frac{\mu_n}{2}\right) \tag{B.3}$$

$$D_{1,n}(\mu_n) = -\sqrt{\gamma_D + \mu_n^2}\sin\left(\frac{\mu_n}{2}\right) \tag{B.4}$$

$$\begin{aligned} A_{2,n}(\alpha_n) = {} & \left[\exp(\alpha_n) + \exp(a\alpha_n)\right]\sqrt{\gamma_D - \alpha_n^2}\cos\left(\frac{a\sqrt{\gamma_D - \alpha_n^2}}{2}\right) + \\ & + \left[\exp(\alpha_n) - \exp(a\alpha_n)\right]\alpha_n \sin\left(\frac{a\sqrt{\gamma_D - \alpha_n^2}}{2}\right) \end{aligned} \tag{B.5}$$

$$\begin{aligned} B_{2,n}(\alpha_n) = {} & \left[\exp(\alpha_n) - \exp(a\alpha_n)\right]\alpha_n \cos\left(\frac{a\sqrt{\gamma_D - \alpha_n^2}}{2}\right) + \\ & - \left[\exp(\alpha_n) + \exp(a\alpha_n)\right]\sqrt{\gamma_D - \alpha_n^2}\sin\left(\frac{a\sqrt{\gamma_D - \alpha_n^2}}{2}\right) \end{aligned} \tag{B.6}$$

$$C_{2,n}(\mu_n) = \sqrt{\gamma_D+\mu_n^2}\cos\left(\frac{\mu_n-a\mu_n}{2}\right)\cos\left(\frac{a\sqrt{\gamma_D+\mu_n^2}}{2}\right)+ \tag{B.7}$$
$$-\mu_n\sin\left(\frac{\mu_n-a\mu_n}{2}\right)\sin\left(\frac{a\sqrt{\gamma_D+\mu_n^2}}{2}\right)$$

$$D_{2,n}(\mu_n) = -\mu_n\sin\left(\frac{\mu_n-a\mu_n}{2}\right)\cos\left(\frac{a\sqrt{\gamma_D+\mu_n^2}}{2}\right)+ \tag{B.8}$$
$$-\sqrt{\gamma_D+\mu_n^2}\cos\left(\frac{\mu_n-a\mu_n}{2}\right)\sin\left(\frac{a\sqrt{\gamma_D+\mu_n^2}}{2}\right)$$

$$A_{3,n}(\alpha_n) = (-1)^n\exp\left(\frac{a\alpha_n}{2}\right)\sqrt{\gamma_D-\alpha_n^2} \tag{B.9}$$

$$B_{3,n}(\alpha_n) = (-1)^n\exp\left(\alpha_n+\frac{a\alpha_n}{2}\right)\sqrt{\gamma_D-\alpha_n^2} \tag{B.10}$$

$$C_{3,n}(\mu_n) = (-1)^n\sqrt{\gamma_D+\mu_n^2}\cos\left(\frac{\mu_n}{2}\right) \tag{B.11}$$

$$D_{3,n}(\mu_n) = (-1)^n\sqrt{\gamma_D+\mu_n^2}\sin\left(\frac{\mu_n}{2}\right). \tag{B.12}$$

Note that if the second sum in equation 9 is started at zero instead of N_α then the coefficients $C_{3,n}$ and $D_{3,n}$ should be multiplied with $(-1)^{N_\alpha}$.

The initial condition, equation (5), can be used to find $R_n(\alpha_n, x_0)$ and $S_n(\mu_n, x_0)$ as:

$$R_n(\alpha_n,x_0) = N_0\frac{F_{i,n}(\alpha_n,x_0)}{\Gamma_\alpha(\alpha_n)^2},\ S_n(\mu_n,x_0) = N_0\frac{G_{i,n}(\mu_n,x_0)}{\Gamma_\mu(\mu_n)^2} \tag{B.13}$$

Where the norm of the modes,

$$\Gamma_\alpha(\alpha_n)^2 = L\frac{\mathrm{e}^{\alpha_n(1+a)}}{\alpha_n}\left[(2-a)\gamma_\mathrm{D}\alpha_n - 2{\alpha_n}^3 + a\gamma_\mathrm{D}\alpha_n\cosh(\alpha_n-\alpha_n a)+\right.$$
$$\left.+2\gamma_\mathrm{D}\sinh(\alpha_n-\alpha_n a)\right] \tag{B.14}$$

and

$$\Gamma_\mu(\mu_n)^2 = \frac{L}{4\mu_n}\left[(2-a)\gamma_D\mu_n + 2{\mu_n}^3 + a\gamma_D\mu_n\cos(\mu_n-a\mu_n) + 2\gamma_D\sin(\mu_n-a\mu_n)\right] \tag{B.15}$$

have been calculated using the equations (7) and (8) in order to simplify as much as possible their form. To obtain equation (B.13) we have used the orthogonality of the modes when integrated over the entire length. The exact expression of equation (B.13) depends on whether x_0 is located in region 1, 2, or 3.